Rab7a activation promotes degradation of select tight junction proteins at the blood-brain barrier after ischemic stroke

Azzurra Cottarelli[1,2,*], Sanjid Shahriar[2,3,**], Ahmet Arac[4,**], Michael Glendinning[1], Mary Claire Tuohy[1], Grace Prochilo[1], Jason B. Neal[1,5], Aimee L. Edinger[6], and Dritan Agalliu[1,2,*]

Departments of [1]Neurology and [2]Pathology and Cell Biology, Columbia University Irving Medical Center, New York, NY, 10032, USA

[3]Wyss Institute for Biologically Inspired Engineering, Boston, MA 02115, USA

[4]Department of Neurology, David Geffen School of Medicine, University of California in Los Angeles, Los Angeles, CA, 90095, USA

[5]Baylor Scott and White Health, Dallas, TX, 75226, USA

[6]Departments of Developmental and Cell Biology and Pharmaceutical Sciences, University of California, Irvine, CA 92697, USA

[**] equal contribution

***Corresponding authors:**

Azzurra Cottarelli, Ph.D. Email: ac4023@cumc.columbia.edu

Dritan Agalliu, Ph.D. Email: da191@cumc.columbia.edu

Lead contact:

Dritan Agalliu, Ph.D. Email: da191@cumc.columbia.edu

SUMMARY (150 words)

The stability of tight junctions (TJs) between endothelial cells (ECs) is essential to maintain blood-brain barrier (BBB) function in the healthy brain. Following ischemic stroke, TJ strand dismantlement due to protein degradation leads to BBB dysfunction, yet the mechanisms driving this process are poorly understood. Here, we show that endothelial-specific ablation of Rab7a, a small GTPase that regulates endolysosomal protein degradation, reduces stroke-induced TJ strand disassembly resulting in decreased paracellular BBB permeability and improved neuronal outcomes. Two pro-inflammatory cytokines, TNFα and IL1β, but not glucose and oxygen deprivation, induce Rab7a activation via Ccz1 in brain ECs *in vitro*, leading to increased TJ protein degradation and impaired paracellular barrier function. Silencing Rab7a in brain ECs *in vitro* reduces cytokine-driven endothelial barrier dysfunction by suppressing degradation of a key BBB TJ protein, Claudin-5. Thus, Rab7a activation by inflammatory cytokines promotes degradation of select TJ proteins leading to BBB dysfunction after ischemic stroke.

KEYWORDS

Rab7a, tight junctions, blood-brain barrier, ischemic stroke, Claudin-5, inflammation, cytokines

INTRODUCTION

The stability of tight junction (TJs) strands formed between endothelial cells (ECs) lining the blood vessels is a critical structural component of the blood-brain barrier (BBB) that, together with low rates of transcellular transport through sparse transcytosis vesicles, restricts the permeability of blood-derived proteins and immune cells into the healthy central nervous system (CNS) to preserve neuronal function (reviewed in [1]). Disintegration of TJ strands occurs in several neurological disorders associated with BBB damage including ischemic stroke, a complex and devastating neurological condition that is the second leading cause of death and the third leading cause of disability worldwide (reviewed in [2-5]). ECs that survive in the peri-infarct region of the brain, but do not maintain BBB properties, facilitate damage to the adjacent parenchyma and exacerbate the clinical prognosis of stroke (reviewed in [1]). Therefore, targeting the molecular pathways that promote stabilization of BBB TJ strands is a highly attractive therapeutic strategy to improve stroke outcomes. Yet, the molecular mechanisms that drive persistent degradation of TJ proteins and loss of BBB integrity *in vivo* at the acute phase of ischemic stroke remain unclear.

During the reperfusion phase of acute ischemic stroke, there is a biphasic increase in BBB permeability that contributes to vasogenic edema, hemorrhage and increased mortality [6-9]. Dynamic imaging studies using green fluorescent protein (GFP)-tagged TJs have found that junctional strands are continuously remodeled at a slow rate in the healthy CNS ECs[10, 11]. However CNS EC junctional strands become highly dynamic and show an increased frequency and number of structural abnormalities (protrusions or gaps) between 48-58 hours after the transient middle cerebral artery occlusion (t-MCAO), a rodent model for ischemic stroke [10]. This phase coincides with increased expression in several pro-inflammatory cytokines, as well as recruitment of immune

63 cells into the CNS (reviewed in [12, 13]), that together contribute to stroke pathophysiology and
64 clinical outcomes [14-16]. These structural BBB TJ abnormalities are not unique to ischemic stroke.
65 They are also found in primary neuroinflammatory CNS diseases to allow immune cell infiltration
66 into the CNS (reviewed in [1]) and have been observed by *in vivo* two photon imaging in
67 experimental autoimmune encephalomyelitis (EAE), a rodent model for human multiple sclerosis
68 prior and throughout the course of the disease [11]. The temporal coincidence of TJ abnormalities
69 and inflammation across multiple CNS diseases emphasizes a critical role for pro-inflammatory
70 mechanisms in driving TJ strand disassembly.
71
72 What mechanisms drive BBB TJ strand disassembly after ischemic stroke? Caveolae have
73 been proposed to promote internalization and degradation of TJ transmembrane proteins such as
74 Claudin-5 and Occludin in CNS and peripheral ECs [17] as well as epithelial cells [18]. However,
75 *Caveolin-1 (Cav-1)* $^{-/-}$ mice lacking caveolae [19, 20] show increased paracellular BBB permeability
76 and infarct size after t-MCAO compared to wild-type mice [10, 21], suggesting that TJ strand
77 disassembly following brain ischemia is not mediated by a caveolar-dependent mechanism.
78 Enhanced endocytotic degradation of distinct BBB transmembrane and intracellular TJ proteins in
79 response to inflammatory cytokines is as a potential mechanism for persistent TJ strand
80 disassembly after ischemic stroke. EC junctional strand protrusions are inhibited by treatment with
81 inhibitors of endocytosis [18], and these structures express the early endosomal marker EEA-1 [11],
82 indicative of a transition into early endosomes. During endocytosis, early endosomes and their
83 cargoes can either be sorted back to the plasma membrane as recycling endosomes, or directed to
84 degradation by maturing into late endosomes/multivesicular bodies that ultimately fuse with
85 lysosomes [22]. Cell membrane trafficking of various cargoes, including transmembrane proteins, is

regulated by small GTPases of the Rab, Arf and Arl families, which cycle between inactive (GDP-bound) and active (GTP-bound) conformational states [23]. The small GTPase Rab7a is critical for cargo sorting into the late endosome, biogenesis of lysosomes and phagocytosis, as well as regulation of substrate degradation, antigen presentation, cell signaling/survival and microbial infection [24, 25].

Although the endolysosomal functions of Rab7 have been extensively studied in mammalian cells, how its activity is regulated is not well understood. In cancer cells, growth factor deprivation increases the fraction of Rab7a associated with membranes and the Rab7a-GTP (active) form, and triggers cell death due to degradation of nutrient transporters essential for survival [26-28]. Conversely, Rab7a inhibition in the setting of growth factor withdrawal promotes cancer cell survival due to recycling of transporters to the cell surface [29, 30]. Regulatory proteins that control Rab7a GTPase activity have been difficult to identify in cells. TBC1D15, has been identified as a putative Rab7a inactivator, since it accelerates GTP hydrolysis by Rab7a *in vitro* and its overexpression disrupts lysosomal morphology and blocks growth factor withdrawal-induced cell death in cancer cells [29]. Ccz1, a guanidine exchange factor (GEF) that acts together with vacuolar fusion protein Mon1, has been shown to promote both Rab7a activation and Rab7a-mediated membrane fusion in yeast [31] and eukaryotic cells [32-35]. Nevertheless, it is unclear whether Mon1/Ccz1 complex activates Rab7a in ECs and the role of Rab7a in EC function has not been fully elucidated. Rab5a and Rab7a regulate VEGFR2 receptor trafficking and the response of ECs to VEGF-A [36] via the Rab effector protein RABEP2 [37]. Recently, the liver kinase B1 (LBK1) has also been identified as a Rab7a effector in ECs that promotes Neuropilin-1 receptor lysosomal trafficking and degradation to inhibit angiogenesis [38]. In lung ECs, Rab4 activation and Rab9

109 inhibition are critical for vascular permeability through regulation of VE-Cadherin (a
110 transmembrane adherens junction protein) localization to cell junctions [39]. Yet, the role of
111 endolysosomal proteins in regulation of BBB function after ischemic stroke has not been explored.
112
113 In this study, we show that endothelial-specific deletion of Rab7a reduces stroke-induced
114 TJ strand disassembly resulting in reduced paracellular BBB permeability and improved neuronal
115 outcomes. TNFα and IL1β, two pro-inflammatory cytokines that are upregulated in the brain after
116 ischemic stroke [13] induce Rab7a activation via Ccz1 in brain ECs *in vitro*, leading to increased TJ
117 protein degradation and impaired paracellular barrier function. In contrast, silencing Rab7a in
118 brain ECs *in vitro* suppresses cytokine-driven barrier dysfunction by preventing degradation of
119 Claudin-5 protein and maintaining its localization at cell-cell junctions. These findings represent
120 a new mechanism by which inflammatory cytokines promote degradation of select TJ proteins via
121 Rab7a activation leading to BBB dysfunction after ischemic stroke.
122
123
124 **RESULTS**
125 **Rab7a is essential in CNS ECs for triggering structural TJ abnormalities and increased**
126 **paracellular BBB permeability 48 hours after t-MCAO.**
127 Studies in T cells and cancer cells have found that Rab7a inhibition is critical to prevent
128 degradation of nutrient transporters and support cell survival [27, 29, 30]. Therefore, we hypothesized
129 that Rab7a activation in ECs may be a critical step to promote degradation of BBB TJ
130 transmembrane proteins after ischemic stroke. To test this hypothesis, we generated a Rab7a-
131 inducible EC knockout mouse strain (*iEC-KO - Rab7a*$^{fl/fl}$*; VEC-Cre*$^{ERT2+/-}$*; eGFP::Claudin5*$^{+/-}$) to

132 delete Rab7a in ECs upon administration of 4-OH-tamoxifen (**Figure 1A, top panel**). These mice
133 also express the eGFP::Claudin5 fusion protein in ECs to visualize TJ strand morphology [10]. We
134 confirmed the efficiency and specificity of Rab7a deletion in ECs by decreased Rab7a protein
135 expression in cortical Lectin (BSL)$^{+}$ blood vessels of *Rab7a iEC-KO* compared to *Rab7a* $^{fl/fl}$ mice
136 (*Rab7a*$^{fl/fl}$*; eGFP-Claudin5*$^{+/-}$; referred as WT) by immunofluorescence (**Figures 1B-C",**
137 **arrowheads**). Rab7a protein was detected equally in other cell types of both WT and *iEC-KO*
138 cortices (**Figures 1B-C", arrows**). We induced ischemic stroke in these mice by performing t-
139 MCAO for 45 minutes and analyzed TJ integrity 48 hours after reperfusion (**Figure 1A, bottom**
140 **panel**), a timepoint at which BBB dysfunction is dominated mainly by TJ strand disassembly [10].
141 WT and *iEC-KO* mice displayed a normal BBB TJ morphology by immunofluorescence for
142 eGFP::Claudin5 and ZO-1 in GLUT1^{+} vessels of the contralateral cortex (**Figure 1D-E"**). In
143 contrast, blood vessels in the ipsilateral somatosensory cortex of WT mice had a high fraction of
144 TJ strands with abnormalities, including gaps [~50%; **Figure 1F-F' (white arrows), H**] and GFP^{+}
145 membrane protrusions [~35%; **Figure 1F-F" (yellow arrowhead**), **I**]. The fractions of TJ strands
146 with gaps and protrusions were significantly lower in the ipsilateral cortex of *iEC-KO* (~18% and
147 20%, respectively) compared to WT mice, but they were not significantly different from those in
148 the contralateral cortexes of both genotypes (**Figure 1G-G", H, I**).
149
150 To determine the effects of Rab7a deletion on total levels of adherens junction (AJ; VE-
151 Cadherin) and TJ [Claudin-5, Occludin, and ZO-1] proteins in ECs after ischemic stroke, lysates
152 were collected from the ipsilateral and contralateral cortices of both genotypes at 48 hours after t-
153 MCAO and assessed via Western blotting (**Figure 2A**). All AJ and TJ proteins were significantly
154 reduced in the ipsilateral cortex of WT mice at 48 hours after t-MCAO, compared to both the WT

155 healthy (t-MCAO sham) and WT contralateral cortex (**Figure 2B-E**). In contrast, Claudin-5,
156 Occludin and ZO-1 protein levels were higher in the ipsilateral cortex of *iEC-KO* mice, and were
157 not significantly different from those in healthy and contralateral *iEC-KO* cortex ($p>0.05$; **Figure**
158 **2B-D**). Importantly, Claudin-5 protein levels were also significantly higher in the ipsilateral cortex
159 of *iEC-KO* compared to WT mice ($p=0.04$), whereas Occludin and ZO-1 protein levels showed
160 higher, but not significantly different, levels in the *iEC-KO* compared to WT ipsilateral cortex
161 [Occludin ($p=0.18$), ZO-1 ($p=0.3$)] (**Figure 2B-D**). Finally, VE-cadherin was significantly reduced
162 in the ipsilateral cortex of WT mice at 48 hours after t-MCAO, compared to both the WT healthy
163 (t-MCAO sham) and WT contralateral cortex, and its levels were not rescued by deletion of Rab7a
164 in ECs (**Figure 2A, E**). Therefore, Rab7a deletion in ECs rescues selectively Claudin-5, a key
165 BBB TJ protein [40], but is less effective for other TJ or AJ proteins after ischemic stroke.
166
167 To determine the effect of Rab7a EC-specific deletion on changes in paracellular BBB
168 permeability after ischemic stroke, we injected biocytin-TMR, an 890 Da dye that preferentially
169 extravasates blood vessels through the paracellular route[10, 11], 48 hours after t-MCAO reperfusion,
170 and analyzed its distribution in seven distinct bregma regions of the brain. WT mice showed an
171 intense biocytin-TMR fluorescence signal in the ipsilateral cortex of all analyzed bregma regions
172 after stroke, with extravascular leakage localized to both the cortex and the striatum in most mice
173 (**Figure 3A, B**). In contrast, the extravascular tracer leakage was less frequent and less extensive
174 in the ipsilateral cortex of all analyzed bregma regions from *iEC-KO* brains (**Figure 3C, D**). There
175 was an overall decrease in the volume of tracer leakage in *iEC-KO* compared to *WT* brains (**Figure**
176 **3E**). In addition, the average area of tracer leakage in each bregma region, representing the fraction
177 of the brain section affected by BBB impairment, and the amount of tracer leakage, measured as

178 fluorescence intensity of the extravasated dye in the parenchyma, were also significantly reduced
179 in *iEC-KO* mice (**Figure 3F, G**). Thus, Rab7a EC-specific deletion rescues structural and
180 functional BBB abnormalities related to TJ disassembly at 48 hours after t-MCAO.
181
182 To determine if Rab7a deletion in ECs affects exclusively paracellular BBB permeability
183 after ischemic stroke, we analyzed the leakage of endogenous serum immunoglobulin G (IgG) as
184 a readout of transcellular transport across the BBB 48 hours after reperfusion. No significant
185 differences in volume, area, or fluorescence intensity of serum IgG leakage were observed between
186 the WT and *iEC-KO* brains (**Figure S1A-G**). Correspondingly, the levels of Cav-1, a protein that
187 mediates transcellular transport across ECs, were comparable in lysates from the ipsilateral and
188 contralateral cortex of WT and *iEC-KO* mice 48 hours after t-MCAO (**Figure S1H, I**), confirming
189 that Rab7a EC-specific deletion did not affect the transcellular BBB leakage after ischemic stroke
190 [10]. Overall, Rab7a EC-specific deletion rescues significantly the paracellular, but not transcellular,
191 BBB permeability at the acute phase after ischemic stroke.
192
193 ***Rab7a iEC-KO* mice show improved neuronal outcomes 48 hours after t-MCAO.**
194 To determine whether the rescue of paracellular BBB permeability after ischemic stroke in
195 *iEC-KO* mice has a neuroprotective effect, we assessed the number of $NeuN^+$ cells, a neuronal
196 marker, in the ipsilateral and contralateral somatosensory cortexes of both genotypes at seven
197 distinct bregma regions. NeuN staining appeared missing or fragmented in the ipsilateral
198 somatosensory cortex of WT mice, but it was markedly rescued in the ipsilateral cortex of *iEC-*
199 *KO* mice (**Figure 4A-I'**). Quantification of the $NeuN^+$ / $DAPI^+$ cell ratio showed a significant
200 reduction in the ipsilateral compared to the contralateral cortex of WT mice (the number of DAPI

201 cells did not change significantly between these two regions) (**Figure 4J**). However, this
202 phenotype was rescued in *iEC-KO* ipsilateral cortex where the cell ratio of $NeuN^+$ / DAPI was
203 comparable to the contralateral cortex in all analyzed bregma regions (**Figure 4J**). Consistent with
204 a larger number of $NeuN^+$ neurons in the cortex after ischemic stroke by immunofluorescence,
205 *iEC-KO* showed fewer neurological deficits with a lower modified Bederson neurological score
206 (0-5) after a series of behavioral tests (forelimb flexion, circling, resistance to lateral push as
207 described in [41]), compared to WT mice 48 hours after t-MCAO (**Figure 4K**). These data
208 demonstrate that *iEC-KO* have an overall improvement in neuronal outcomes after t-MCAO, likely
209 due to a smaller stroke volume (**Figure 3E**).
210
211 To examine if the rescue in structural and functional paracellular BBB impairment
212 observed in *iEC-KO* mice after ischemic stroke reduces local inflammation, we analyzed myeloid
213 cells (activated microglia and infiltrating macrophages) and resting microglia in the stroke core,
214 border and contralateral cortex of both genotypes 48 hours after t-MCAO (**Figure S2A, E**; yellow
215 outlined area and green boxed regions 1-3). Resting microglial cells ($Iba1^+$ $CD68^-$ cells with
216 ramified branches) were found outside the BBB leakage area both at the stroke border and in the
217 contralateral cortex (Figure **S2C-D'", G-H'"**; white arrows). In contrast, myeloid cells ($Iba1^+$
218 $CD68^+$ cells with ameboid morphology representing both activated microglia and macrophages)
219 were found in the stroke core and border within the BBB leakage area in both *WT* and *iEC-KO*
220 cortexes (**Figure S2B-C'", F-G'"**; white arrowheads within the red border). The ratio of $CD68^+$
221 $Iba1^+$ over total $Iba1^+$ cells was similar in the cortex of both genotypes at all analyzed bregma
222 regions with no significant differences between the two genotypes (**Figure S2I**). Although
223 somewhat paradoxical, the similar local inflammatory changes found in both WT and *iEC-KO*

224 cortexes in the acute phase (48 hours) of ischemic stroke could be a consequence of a partial, rather
225 than a complete, rescue in BBB permeability in mutant mice since Rab7a EC-specific deletion
226 rescues significantly the paracellular, but not transcellular, BBB permeability at the acute phase of
227 disease.
228
229 **Pro-inflammatory cytokines, TNFα and IL1β, but not glucose and oxygen deprivation,**
230 **induce Rab7a activation via upregulation of Ccz1 in brain ECs *in vitro.***
231 Rab7a cycles between inactive (GDP-bound) and active (GTP-bound) states to regulate
232 various cell biological processes [24, 25]. Rab-interacting lysosomal protein (RILP) binds selectively
233 to Rab7-GTP and recruits the dynein-dynactin motor complex to facilitate vesicle movement
234 toward the minus end of microtubules [42]. The N terminus region of RILP is required to recruit
235 dynein motors, but not for Rab7-GTP binding; therefore an N-terminal truncation of RILP can be
236 used to assess Rab7 activation in cells [29]. To investigate the molecular mechanisms responsible for
237 Rab7a activation in ischemic stroke, we cultured primary mouse brain ECs (mBECs) *in vitro* under
238 conditions of either glucose and oxygen deprivation (OGD), or inflammation, and quantified the
239 amount of GTP-bound Rab7a by using a GST-RILP fusion protein to pull down selectively the
240 active protein from the cell lysate (**Figure 5A**). First, we tested whether the ischemic environment
241 in stroke promotes Rab7a activation by growing mBECs under OGD conditions for 48 hours.
242 Surprisingly, both the total and GTP-bound Rab7a levels were decreased significantly after 48
243 hours of OGD treatment (**Figure 5G-I**), suggesting that ischemic conditions do not activate Rab7a
244 protein. The lower levels of Rab7a in OGD conditions were not associated with increased cell
245 death (data not shown). Since ischemic stroke induces inflammation[13], we then tested the ability
246 of several pro-inflammatory cytokines to induce Rab7a activation. Treatment with a combination

247 of TNFα and IL1β did not increase the total amount of Rab7a, but produced a trend, albeit non-
248 significant, towards increased GTP-bound Rab7a levels after 24 hours (**Figure 5B-D**). After 48
249 hours of TNFα and IL1β treatment, Rab7a-GTP levels were significantly increased without a
250 change in the total Rab7a levels (**Figure 5B, E, F**). Three other pro-inflammatory cytokines that
251 are upregulated after ischemic stroke, IL-21 [43], CCL2 [44] and IL-17A [45], had no effect on either
252 total or activated Rab7a levels in mBECs at 48 hours after treatment (**Figure S3**), indicating that
253 select pro-inflammatory cytokines promote Rab7a activation in primary mBECs.
254
255 Next, we examined expression of Ccz1, a GEF that acts together with vacuolar fusion
256 protein Mon1 to promote both Rab7a activation and Rab7a-mediated membrane fusion in yeast [31]
257 and eukaryotic cells [32-35]. Ccz1 expression was significantly increased in mBECs 24 hours after
258 TNFα and IL1β exposure. However, this effect was transient and Ccz1 protein returned to control
259 levels at 48 hours after cytokine treatment (**Figure 5J, K**). Thus, TNFα and IL1β induce expression
260 of Ccz1 in mBECs within 24 hours, which likely results in Rab7a activation peaking between 24-
261 48 hours to promote degradation of TJ proteins.
262
263 **Rab7a knockdown reduces cytokine-driven EC barrier dysfunction *in vitro* by preventing**
264 **degradation of Claudin-5 protein.**
265 To investigate the downstream effect of Rab7a activation on brain EC barrier integrity at
266 the cell biological level, we generated Rab7a knockdown primary mBECs via transfection of
267 stealth RNAi duplexes targeting the *Rab7a* mRNA transcript. We verified the efficiency of Rab7a
268 protein downregulation by immunofluorescence and Western blotting, and found that Rab7a
269 expression was decreased by 75% in mBECs transfected with the siRNA (siRab7a) compared to

270 those transfected with a scrambled siRNA (siCTRL). This knockdown efficiency was observed in
271 the presence and absence of TNFα and IL1β (**Figure S4A-F**). We examined whether Rab7a
272 knockdown affected the levels of other proteins in the endolysosomal pathway, such as the early
273 endosomal marker EEA-1 and the lysosomal marker LAMP-1 by Western blotting. We confirmed
274 that EEA-1 and LAMP-1 protein levels were not different in both siCTRL- and siRab7a-
275 transfected mBECs with or without cytokine treatment (**Figure S4E, G, H**). Since Rab7a activity
276 maintains lysosome mass, we quantified the lysosome mass per cell in both siCTRL- and siRab7a-
277 transfected mBECs after immunostaining for the pH sensor Lysotracker. The lysosome mass per
278 cell was similar between siCTRL and siRab7a treatments with or without cytokine treatment
279 (**Figure S4I-M**). Together, these data demonstrate that Rab7 knockdown does not affect other
280 endolysosomal proteins and the lysosome mass in mBECs.
281
282 Since Rab7a plays a critical role in autophagy (reviewed in [46]), we examined whether
283 Rab7a knockdown affected expression of the two autophagy proteins Atg5 and p62 under basal
284 and inflammatory conditions in mBECs. Under basal conditions, the levels of Atg5 and p62
285 proteins were similar in both siCTRL- and siRab7a-transfected mBECs (**Figure S5A-C**). As
286 expected, the Atg5 and p62 protein levels were upregulated under inflammatory conditions in both
287 siCTRL- and siRab7a-transfected mBECs (**Figure S5A-C**). Moreover, p62 levels were
288 significantly higher in siRab7a-transfected mBECs after cytokine treatment, suggesting that Rab7a
289 knockdown induced p62 accumulation in mBECs (**Figure S5A-C**), likely due to reduced
290 autophagy.
291
292 To determine if Rab7a knockdown rescues cytokine-mediated increase in mBEC

293 paracellular permeability we analyzed the transendothelial electrical resistance (TEER) in
294 siCTRL- and siRab7a-transfected cells after cytokine treatment. In the absence of cytokines,
295 siRab7a-transfected mBECs show a decreased basal TEER compared to siCTRL-transfected cells
296 (**Figure 6A-C**). Treatment of siCTRL-transfected mBECs with TNFα and IL1β for 48 hours
297 significantly reduced the TEER. However, this cytokine mediated disruption was mitigated in
298 siRab7a-transfected mBECs (**Figure 6A-C**). To investigate which TJ proteins are regulated by
299 Rab7a in mBECs, we examined expression and subcellular localization of TJ proteins (Claudin-5,
300 Occludin and ZO-1) at 48 hours after cytokine addition. Cytokine treatment significantly reduced
301 the levels of Claudin-5 and ZO-1, but not Occludin, proteins in mBECs. Furthermore, transfection
302 with siRab7a rescued cytokine-induced degradation of Claudin-5, but not ZO-1, protein levels in
303 mBECs (**Figure 6D-G**).
304
305 At the basal level, siRab7a-transfected mBECs showed irregular cell junctions compared
306 to siCTRL-transfected cells (**Figure 6H-H", J-J"**), a phenotype resembling the lack of ZO-1/ZO-
307 2 in epithelial cells [47], although ZO-1 protein co-localized with Claudin-5. This observation likely
308 explains the lower TEER seen with siRab7a-treated mBECs under basal conditions (**Figure 6A**).
309 Treatment with inflammatory cytokines induced the appearance of gaps and protrusions in
310 Claudin-5^{+} cell junction strands in siCTRL-treated mBECs, and loss of ZO-1 protein from most
311 cell junctions (**Figure 6I-I"**). Although cytokine-treated Rab7a-deficient mBECs show an
312 exacerbated jagged cell junction phenotype due to the absence of ZO1, very few gaps and
313 protrusions in Claudin-5^{+} strands were observed after exposure to pro-inflammatory cytokines
314 (**Figure 6K-K"**). Cytokine treatment, however, downregulated potently ZO-1 protein in both
315 control and siRab7a-transfected mBECs (**Figure 6I-I", K-K"**), indicating that Rab7a knockdown

316 has very selective effects on degradation of distinct TJ proteins.

317

318 Since Cav-1 protein has been shown to regulate Claudin-5 protein levels in mBECs after
319 exposure to inflammatory chemokines (e.g. CCL2)[17], we examined its levels and the caveolar-
320 mediated transcytosis in Rab7a knockdown cells. Cav-1 protein levels were increased in primary
321 BECs after exposure to TNFα and IL1β independently of Rab7a levels (**Figure S5I-J**). In addition,
322 we performed an albumin-594 uptake assay to measure Caveolin-1-dependent transcellular
323 transport, and confirmed that albumin-594 uptake was equally increased in siCTRL- and siRab7a-
324 transfected mBECs upon treatment with cytokines (**Figure S5D-H**). Therefore, the rescue of
325 Claudin-5 degradation with pro-inflammatory cytokines following Rab7a knockdown in mBECs,
326 is not due to changes in Caveolin-1 protein levels and caveolar-mediated transport. In conclusion,
327 the *in vivo* and *in vitro* data demonstrate that Rab7a is necessary for cytokine-induced degradation
328 of select BBB TJ proteins (e.g. Claudin-5) and enhanced paracellular permeability in mouse brain
329 endothelial cells, but is not involved in the increased caveolar transcellular transport in brain ECs.

330

331

332 **DISCUSSION**

333 The disassembly of cell junctions due to persistent degradation of adherens and tight junction
334 proteins has long been considered as the main contributor to increased BBB permeability in
335 multiple neuropathological conditions, including ischemic stroke. However, the cell biological
336 mechanisms driving this process are still debated. OGD, perhaps the most obvious trigger, has
337 been proposed to promote junctional protein degradation through activation of several proteases
338 [48, 49]. Surprisingly, we find that OGD does not activate Rab7a in primary brain endothelial cells,

339 suggesting that OGD-induced junctional protein degradation does not require Rab7a activation.
340 Our findings support previous studies that two pro-inflammatory cytokines, IL-1β and TNF-α,
341 which are upregulated in stroke tissue between 24-48 hours after reperfusion and coincide with
342 immune cell infiltration into the CNS (reviewed in [12, 13]), induce internalization and degradation
343 of BBB TJ proteins [17, 18]. We further demonstrate that IL-1β and TNF-α, but not other pro-
344 inflammatory cytokines found in the stroke milieu (e.g. CCL2, IL-21, IL-17A), induce Rab7a
345 activation likely via GEF Ccz1 [31-33], which then drives degradation of selective BBB cell junction
346 proteins. Other pro-inflammatory cytokines/chemokines that have been implicated in BBB
347 dysfunction such as IL-17A, IL-21 and CCL2 may promote TJ degradation through Rab7a-
348 independent mechanisms, since they cannot activate Rab7a in primary brain ECs. Therefore, pro-
349 inflammatory cytokines likely mediate BBB TJ degradation at the acute phase of ischemic stroke
350 through both Rab7a-dependent and -independent mechanisms.
351
352 Cav-1 has been previously implicated in tight junction transmembrane protein
353 internalization and degradation [17, 18, 48]. Our data demonstrate that Rab7a-mediated TJ rescue is not
354 accompanied by changes in Caveolin-1 protein levels or caveolar-mediated transcellular
355 permeability *in vitro* and *in vivo* (**Figures S1I, S5I**). Moreover, the pro-inflammatory chemokine
356 CCL2 is unable to induce Rab7a activation in primary brain endothelial cells (**Figure S3D-F**),
357 although it has been shown to promote Caveolin-1-mediated internalization of Claudin-5 in the
358 bEnd3.0 cell line [17]. Although we cannot exclude the possibility that Caveolin-1-dependent cargo
359 sorting is a putative mechanism of junctional protein degradation under some conditions, it is likely
360 not the predominant mechanism by which inflammation-mediated degradation of cell junction
361 proteins occurs in the setting of acute ischemic stroke. Thus, the cellular mechanisms of BBB TJ

362 protein degradation are context dependent and likely differ across distinct neurological diseases.

363

364 Overall our findings *in vivo* and *in vitro* suggest a model for how the state of Rab7a
365 activation in brain ECs regulates recycling and degradation of BBB TJ proteins under healthy and
366 disease states (**Figure 6L**). We propose that under physiological conditions, similar levels of active
367 and inactive Rab7a protein levels regulate a constant internalization, recycling and degradation of
368 transmembrane adherens and tight junction proteins, in order to maintain their steady-state levels
369 at cell junctions (**Figure 6L, left panel**). When ECs are exposed to a subset of pro-inflammatory
370 cytokines (e.g. TNFα and IL1β), such as under acute conditions of ischemic stroke, they
371 upregulate Ccz1 expression, a GEF which promotes Rab7a activation [31-33]. Rab7a hyperactivation
372 results in an imbalance of the endolysosomal pathway towards degradation rather than recycling,
373 drives cell junction transmembrane proteins to the lysosomes, and triggers tight junction
374 dismantlement which further exacerbates paracellular BBB permeability (**Figure 6L, right panel**).
375 Our study identifies a new molecular mechanism controlling EC junctional integrity in diseased
376 BBB, and establishes Rab7a as a key regulator of TJ protein turnover via the endolysosomal
377 pathway in CNS inflammation. These findings have implications for not only ischemic stroke, but
378 potentially other neurological disorders characterized by inflammation and BBB dysfunction. For
379 example, in EAE, structural BBB TJ abnormalities precede the onset of disease and persist
380 throughout the course of EAE to allow immune cell infiltration into the CNS [11], emphasizing a
381 critical role for pro-inflammatory mechanisms in driving TJ strand disassembly. Based on our
382 findings in this study, we postulate that early and persistent Rab7a activation due to pro-
383 inflammatory cytokines Il-1β and TNF-α may likely drive degradation of BBB TJ transmembrane
384 proteins in EAE leading to early and persistent BBB leakage [11].

385

386 The proposed mechanism by which Rab7a activation triggers degradation of junctional
387 proteins to promote persistent dismantlement of cell junctions implies a potential lack of
388 selectivity, since the endolysosomal degradation is a fundamental cell biological process.
389 However, our genetic loss-of-function data suggest that Rab7a elimination both *in vivo* and *in vitro*
390 rescues both the levels and localization of selective transmembrane cell junction proteins such as
391 Claudin-5, a key BBB TJ protein. In contrast, Rab7a elimination does not rescue significantly the
392 levels of Occludin (a transmembrane TJ protein) and ZO-1 (an intracellular TJ component that
393 anchors transmembrane junction proteins to the actin cytoskeleton). This discrepancy could result
394 because either low levels of Rab7a may be sufficient to degrade Occludin and ZO-1 protein, or
395 their degradation could be mediated by a Rab7a-independent mechanism under inflammatory
396 conditions. Moreover, Rab7a knockdown has no effect on the levels of Caveolin-1 or Slc2a1 (Glut-
397 1), which are both integral membrane proteins. A possible explanation is that TNFα, which
398 activates Rab7a, also promotes the formation of actin stress fibers [50] that further induce
399 disassembly and internalization of junctional proteins [51]. In conclusion, our findings represent a
400 new mechanism by which inflammatory cytokines promote degradation of select TJ proteins via
401 Rab7a activation, leading to BBB dysfunction after ischemic stroke. Recently, a small chemical
402 molecule (CID 1067700) has been identified as a potent inhibitor of Rab7a-GTPase activity with
403 (K_i) values that range from 12.90-19.70 nM [52]. Future studies will determine whether this
404 compound can reduce or prevent BBB breakdown and disease outcomes after ischemic stroke.

405

406

407 **ACKNOWLEDGEMENTS**

We thank Martin Hsu (UNC) and Julian Smith (University of Washington) for initial help with the project and the generation of *Rab7a-iECKO* mice, respectively; Tyler Cutforth for scientific and editorial feedback on this project. A.C., S.S., M.G., G.P. and D.A. are supported by grants from the National Eye Institute (R01EY033994), National Heart Lung and Blood Institute (R61HL159949), National Institute of Aging (RF1AG078352), National Institute of Neurological Disorders and Stroke (R21NS130265), the Leducq Foundation (FDNLEDQ 15CVD 02) and in part by a gift donation from the Ju Foundation. Development of the Rab floxed mouse was supported by a grant from the National Cancer Institute to ALE (K08 CA100526).

AUTHOR CONTRIBUTIONS

Conceptualization: A.C., D.A.; Methodology: A.C., S.S., A.A., M.G., G.P., J.N., M.C.T., A. L. E., D.A.; Formal analysis: A.C., S.S., M.G., M.C.T.; Investigation: A.C., S.S., A.A., M.G., M.C.T.; Resources: A.L.E, D.A.; Data curation: A.C., S.S., M.G., M.C.T.; Writing - original draft: A.C., D.A.; Writing - review & editing: A.C., S.S., A.A., M.C.T., A.L.E, M.C.T., D.A.; Visualization: A.C.; Supervision: D.A., Project administration: D.A., Funding acquisition: D.A.

DECLARATION OF INTEREST

The authors declare no competing or financial interests relevant to the subject matter in this contribution.

FIGURES AND FIGURE LEGENDS

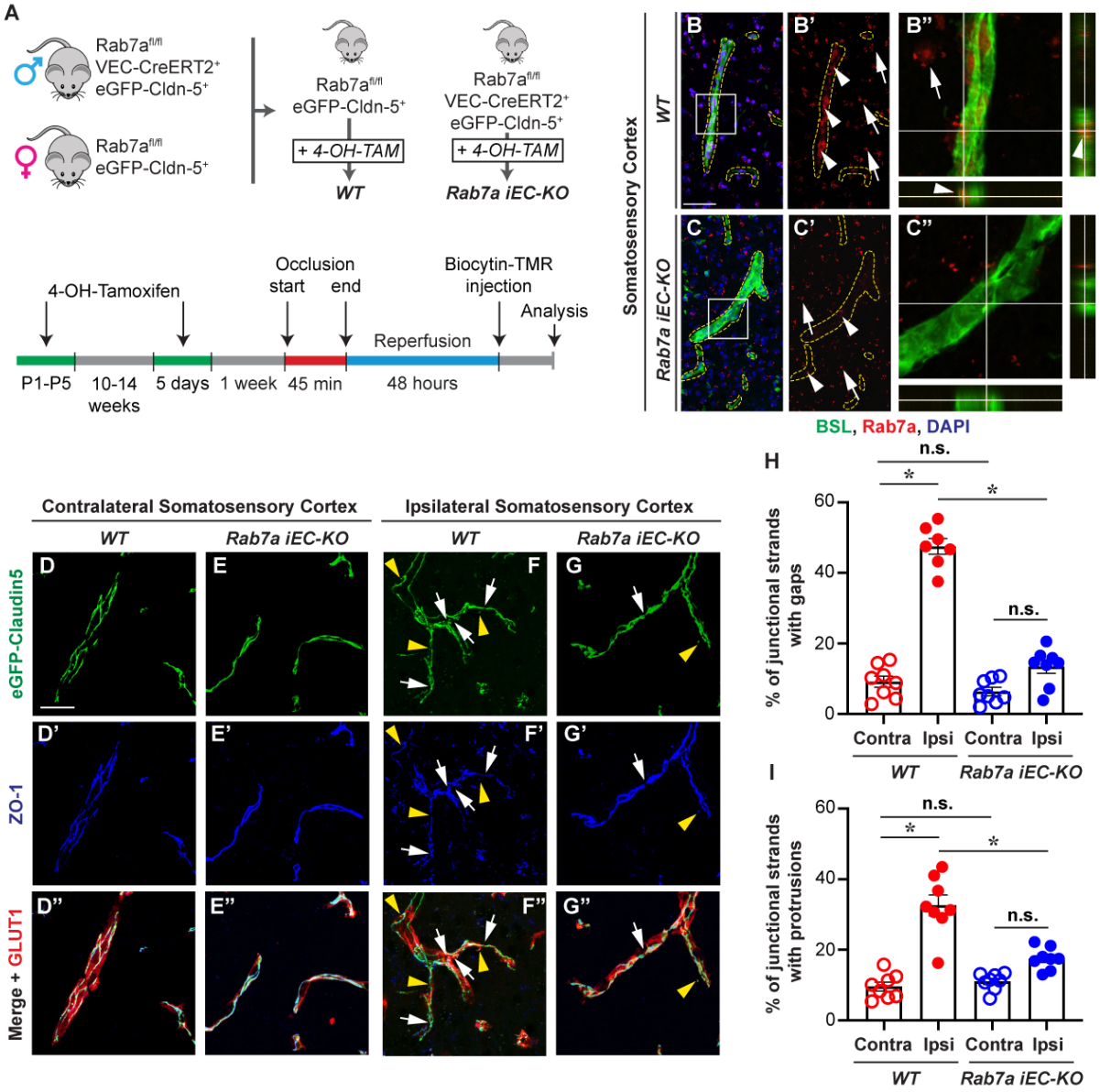

Figure 1. Rab7a is essential for structural abnormalities found in BBB tight junctions 48 hours after t-MCAO.

(**A**) Diagrams showing the breeding strategy to generate the inducible endothelial Rab7a knockout (*Rab7a iEC-KO*) mice and the experimental setup to analyze the paracellular blood-brain barrier (BBB) permeability after t-MCAO. (**B-C"**) Immunofluorescence images for Griffonia

437 (Bandeiraea) Simplicifolia Lectin I (BSL, green), Rab7a (red) and DAPI (blue) in the cortex of
438 healthy WT (**B-B”**) and *Rab7a iEC-KO* (**C-C”**) mice. Cortical vessels are delineated by yellow
439 dotted lines (**B’**, **C’**). Boxed areas are magnified in the orthogonal view images on the right (**B”**,
440 **C”**). Arrowheads indicate endothelial Rab7a, arrows indicate non-endothelial Rab7a. There is very
441 little residual Rab7a protein in ECs of mutant mice. Scale bar: 30 μm. (**D-G”**)
442 Immunofluorescence images for eGFP-Claudin5 (green), ZO-1 (blue) and BSL (red) in the
443 contralateral (**D-E”**) and ipsilateral (**F-G”**) cortex of WT and *Rab7a iEC-KO* mice 48 hours after
444 t-MCAO. White arrows point to gaps, yellow arrowheads show protrusions in BBB tight junction
445 strands. Scale bar: 25 μm. (**H**, **I**) Quantification of junction gaps (**H**) and protrusions (**I**) in the
446 contralateral and ipsilateral cortex of *WT* and *Rab7a iEC-KO* mice 48 hours after t-MCAO. Each
447 dot represents an animal (n=7-8 mice / group). Data are means ± s.e.m. *: $p<0.05$; n.s.: $p>0.05$;
448 one-way ANOVA with post-hoc Tukey’s correction.
449

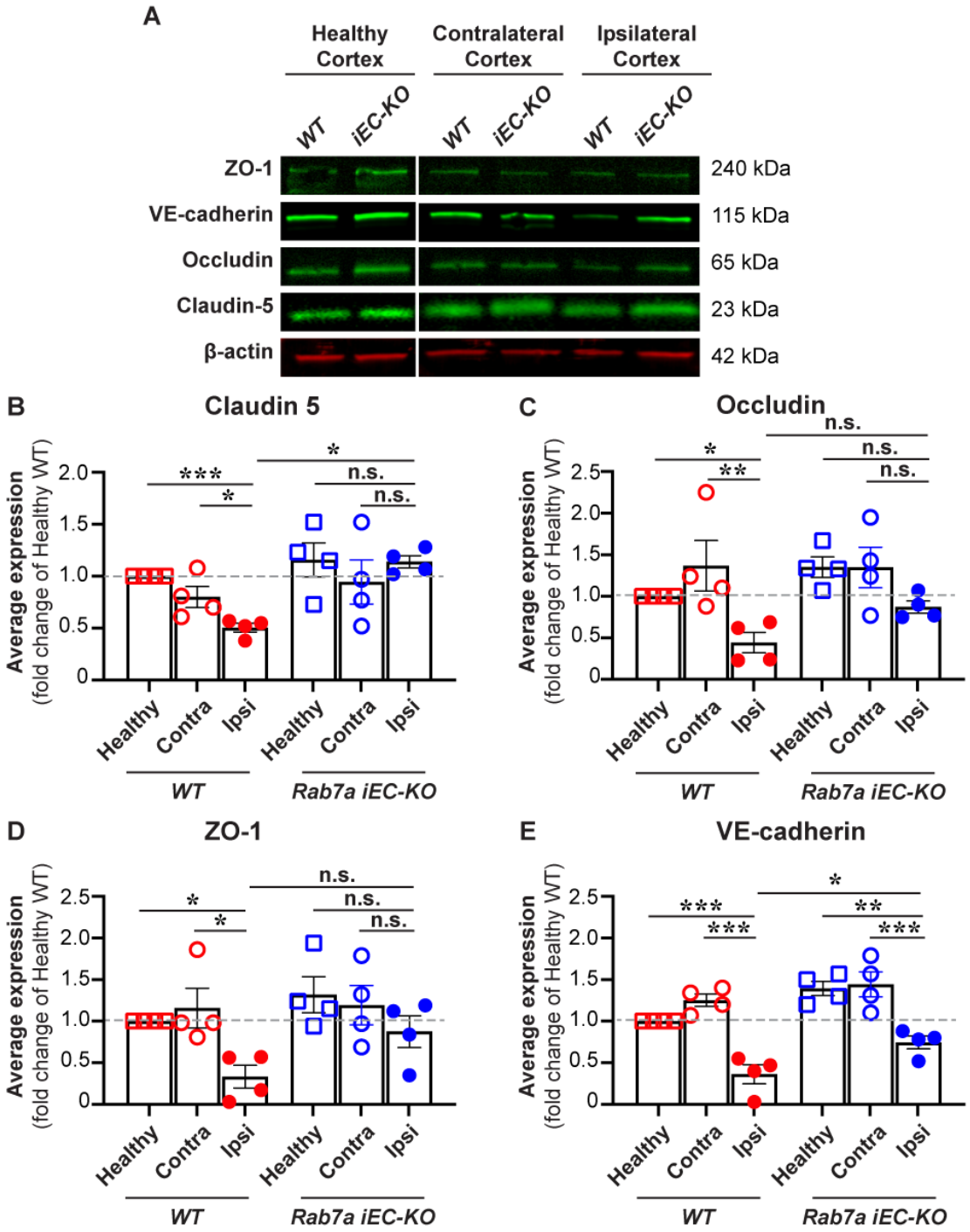

Figure 2. Rab7a regulates degradation of selective BBB TJs 48 hours after t-MCAO. (**A**) Western blots for BBB junctional proteins ZO-1, VE-cadherin, Occludin and Claudin-5 and β-actin (control) of brain lysates collected from either the healthy or contralateral and ipsilateral ischemic cortex of *WT* and *Rab7a iEC-KO* mice 48 hours after t-MCAO. The respective molecular

weights for each protein are shown on the right. (**B-E**) Quantification of Claudin-5, Occludin, ZO-1 and VE-cadherin protein levels in either healthy, contralateral or ipsilateral ischemic brain lysates of *WT* and *Rab7a iEC-KO* mice 48 hours after t-MCAO. Each dot represents an animal (n=4 mice / group). Data are means ± s.e.m and normalized to WT healthy levels. ***: p<0.001; **: p<0.01; *: p<0.05; n.s.: p>0.05; one-way ANOVA with post-hoc Tukey's correction.

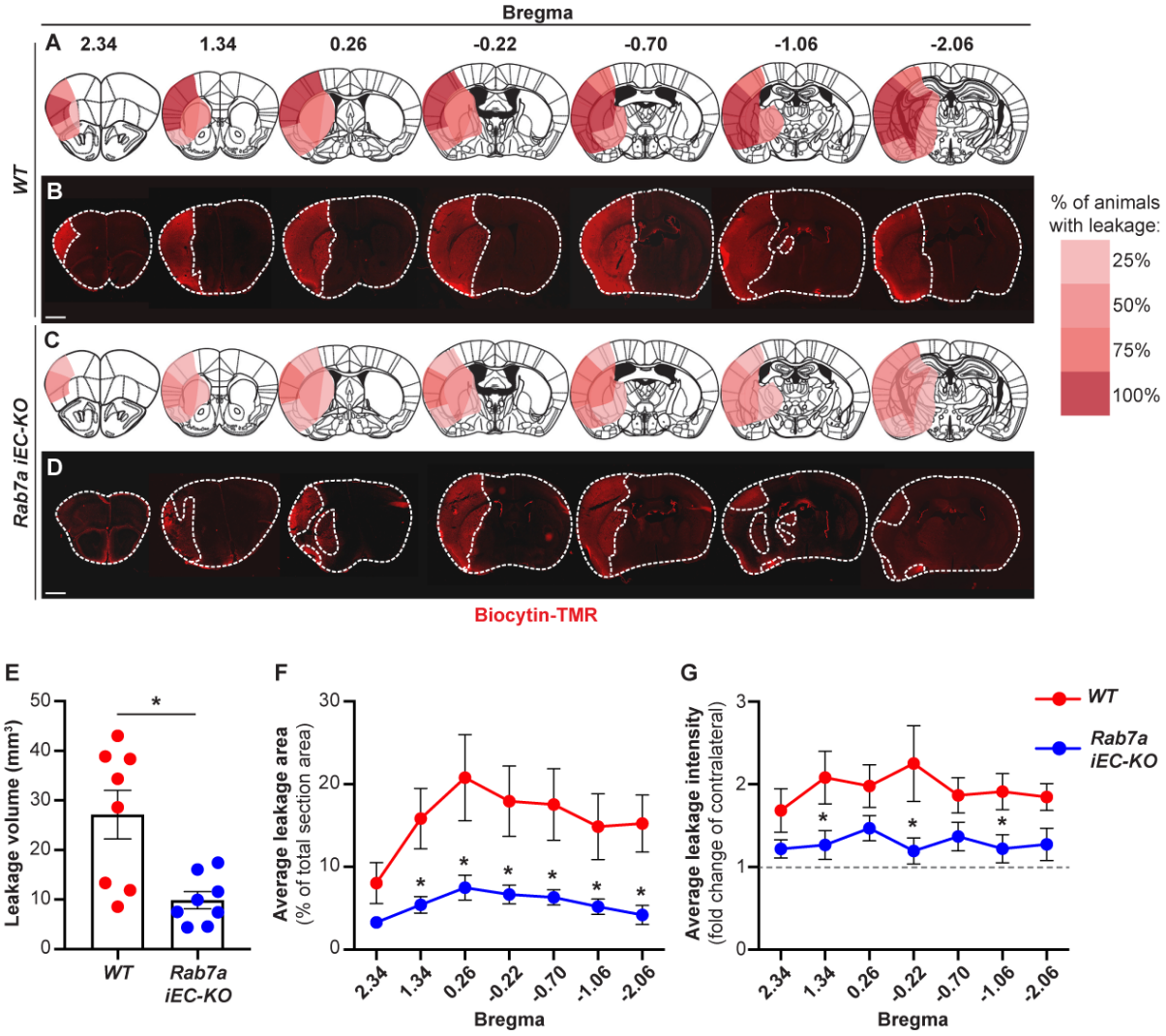

Figure 3. *Rab7a iEC-KO* mice show a partial rescue in the paracellular BBB permeability 48 hours after t-MCAO.

464 (**A-D**) Fluorescent micrographs and heatmaps showing biocytin-TMR tracer extravasation in
465 seven distinct brain regions in WT (**A, B**) and *Rab7a iEC-KO* (**C, D**) mice 48 hours after t-MCAO
466 (biocytin-TMR was injected 30 minutes before analysis). Dotted lines outline the border of the
467 brain section and the leakage area. The heatmaps show the fraction of animals displaying BBB
468 leakage in each region represented as a scale (0-100%) of red hues. (**E**) Quantification of biocytin-
469 TMR leakage volume in the brain of WT and *Rab7a iEC-KO* mice 48 hours after t-MCAO. n=8
470 animals/group. Data are means ± s.e.m. *: $p<0.05$; Student's t-student. (**F**) Quantification of
471 biocytin-TMR leakage area in each bregma region from WT and *Rab7a iEC-KO* mice 48 hours
472 after t-MCAO. Each dot represents the average of n=8 animals / group. Data are means ± s.e.m. *:
473 $p<0.05$; one-way ANOVA with post-hoc Tukey's correction. (**G**) Quantification of the intensity
474 of biocytin-TMR leakage in the ipsilateral cortex of each bregma region from WT and *Rab7a iEC-*
475 *KO* mice 48 hours after t-MCAO. The dotted line represents the average fluorescence intensity in
476 the contralateral cortex. Each dot represents the average of n=8 animals. Data are means ± s.e.m.
477 *: $p<0.05$; one-way ANOVA with post-hoc Tukey's correction. Please see also **Figure S1**.
478

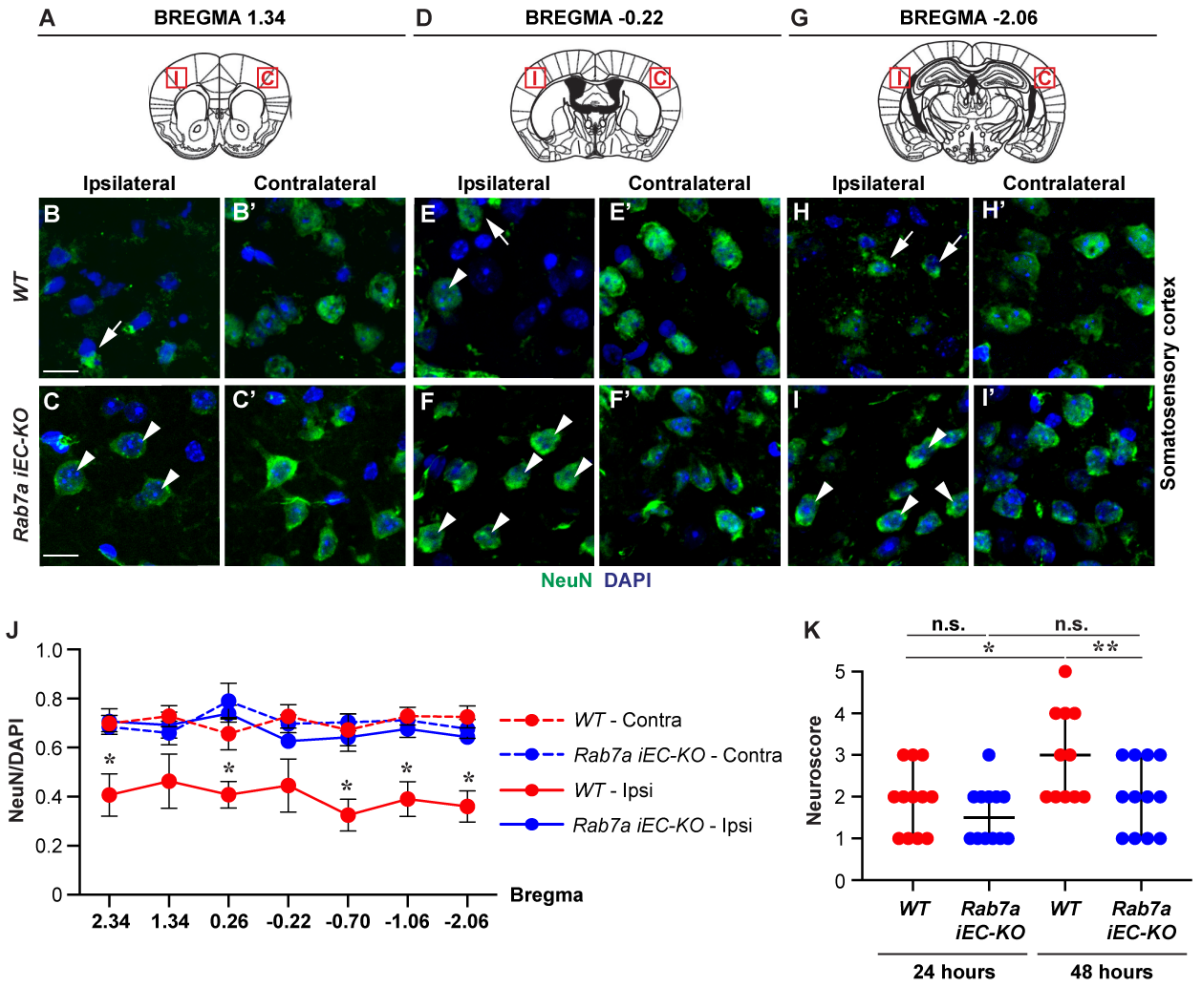

Figure 4. *Rab7a iEC-KO* mice show improved neuronal survival and neurological score 48 hours after t-MCAO.

(**A-I'**) Immunofluorescence analysis for NeuN (green) and DAPI (blue) in the contralateral and ipsilateral cortex of WT and *Rab7a iEC-KO* mice 48 hours after t-MCAO. (**A, D, G**) Diagrams illustrate the bregma regions and the red boxes outline the cortical area shown in each micrograph in **B-I**'. (**B-I'**) White arrows indicate abnormal and white arrowheads indicate normal NeuN staining in the ipsilateral cortex. Scale bar: 25 µm. (**J**) Quantification of the fraction of viable neurons (NeuN/DAPI ratio) in the contralateral (dotted lines) and ipsilateral (solid lines) cortexes in seven bregma regions of WT and *Rab7a iEC-KO* mice 48 hours after t-MCAO. Each dot represents the average of n=8 animals / group. Data are means ± s.e.m. *: $p<0.05$; one-way

490 ANOVA with post-hoc Tukey's correction. (**K**) Analysis of neurological score in WT and *Rab7a*
491 *iEC-KO* mice 24 and 48 hours after t-MCAO. Each dot represents one animal (n=8 mice / group).
492 Data are medians ± 95% C.I. *: $p<0.05$; **: $p<0.01$; Kruskal-Wallis one-way ANOVA. Please see
493 also **Figure S2**.
494

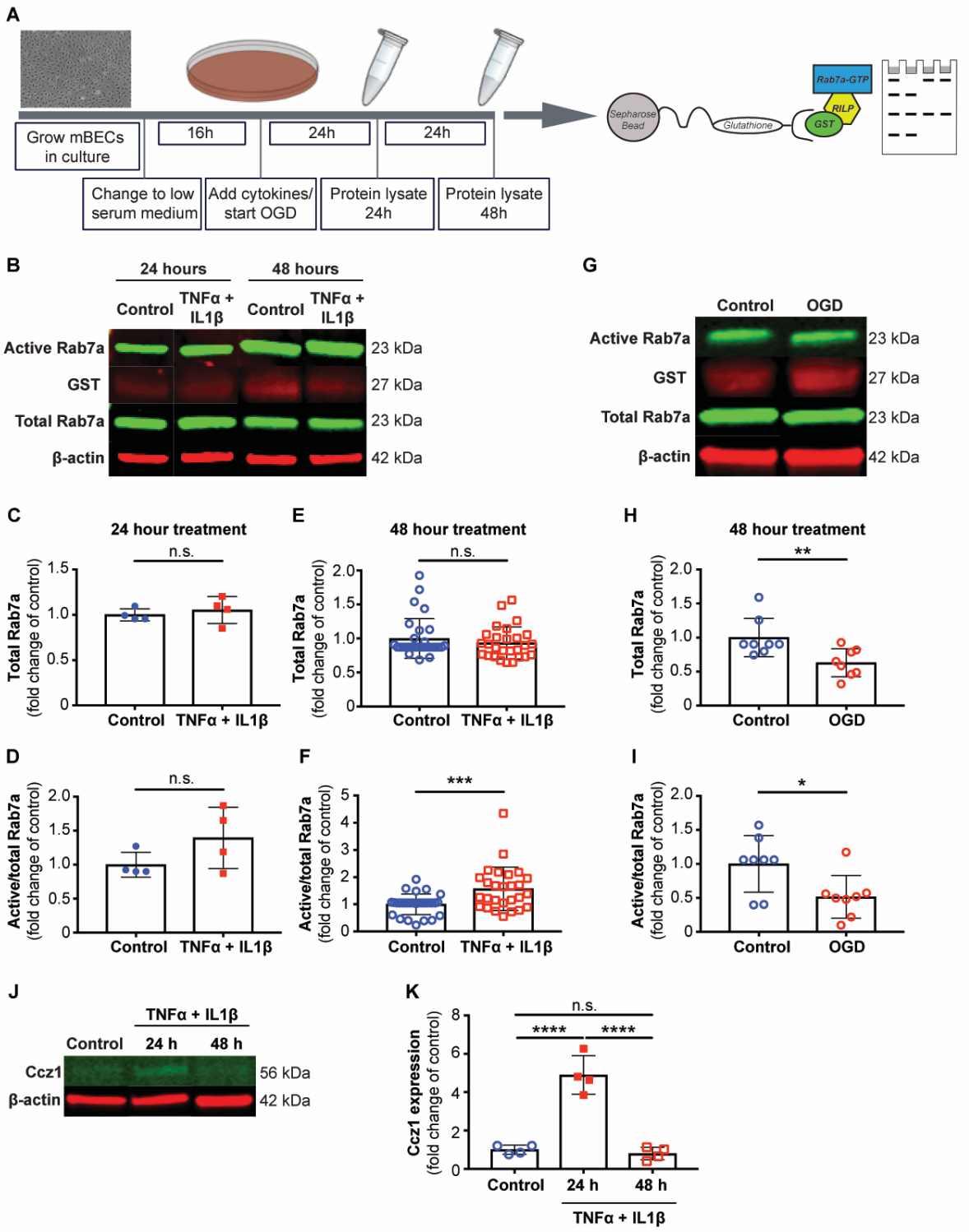

495

496 **Figure 5. Proinflammatory cytokines TNFα and IL1β induce Rab7a activation in mouse**

497 **brain endothelial cells via upregulation of Ccz1.**

498 (**A**) Schematic diagram of the experimental setup. Primary mouse brain endothelial cells (mBECs)
499 are grown to confluence and switched to low-serum media overnight prior to addition of pro-
500 inflammatory cytokines (TNFα, IL-1β; 10 ng/mL). Protein lysates are collected after 24 or 48
501 hours of cytokine treatment. Rab7a-GTP is pulled down using a GST-RILP fusion protein that
502 binds glutathione immobilized on sepharose beads. Western blotting is then used to detect both
503 Rab7a and Rab7a-GTP protein levels. (**B**) Western blot of active and total Rab7a proteins in
504 mBECs treated with TNFα and IL1β for either 24 or 48 hours and untreated control cells. GST and
505 β-actin are used to normalize active Rab7a and total Rab7a levels, respectively. The molecular
506 weight of each protein is shown on the right. (**C-F**) Quantification of total (**C, E**) and active (**D,**
507 **F**) Rab7a levels in mBECs treated with TNFα and IL1β for 24 hours (**C, D**) and 48 hours (**E, F**)
508 and untreated cells. Each dot represents an independent experiment. Data are means ± s.e.m. (**F**)
509 ***: $p<0.005$; Student's t-test. (**G**) Western blot for active and total Rab7a in mBECs grown in
510 oxygen and glucose deprivation (OGD) conditions for 48 hours and untreated control cells. GST
511 and β-actin are used to normalize active Rab7a and total Rab7a levels, respectively. The molecular
512 weight of each protein is shown on the right. (**H, I**) Quantification of total (**H**) and active (**I**) Rab7a
513 levels in mBECs grown in OGD conditions for 48 hours and control cells. Each dot represents an
514 independent experiment. Data are means ± s.e.m.; **: $p<0.01$; *: $p<0.05$; n.s. $p>0.05$ Student's t-
515 test. (**J**) Western blot for Ccz1 in mBECs treated with TNFα and IL1β for 24 and 48 hours and
516 untreated cells. (**K**) Quantification of Ccz1 protein levels in mBECs treated with TNFα and IL1β
517 for 24 and 48 hours and untreated cells. Each dot represents an independent experiment. Data are
518 means ± s.e.m. ****: $p<0.001$; one-way ANOVA with post-hoc Tukey's correction. Please see
519 also **Figure S3**.
520

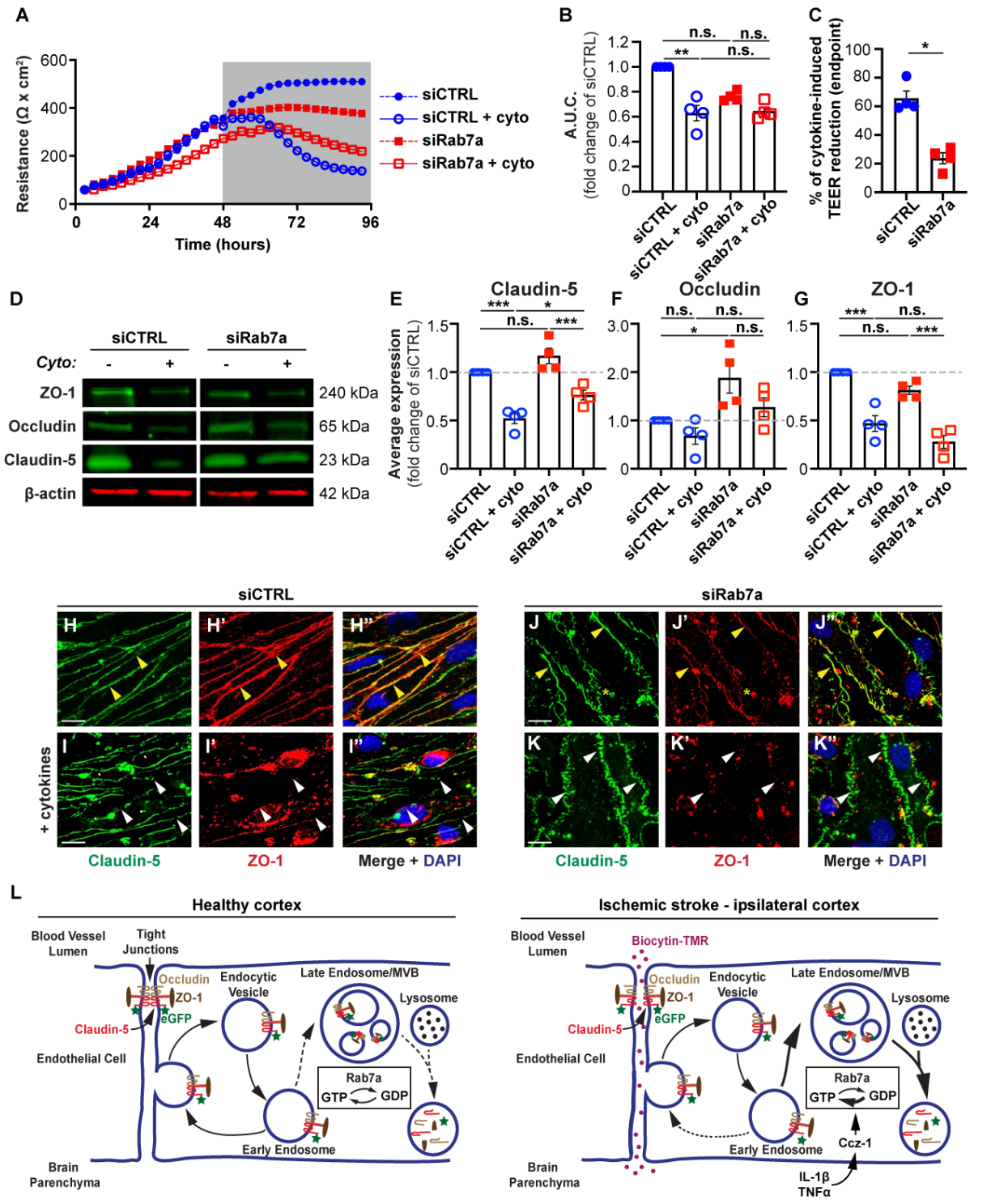

Figure 6. Rab7a knockdown reduces cytokine-driven EC barrier dysfunction by preventing degradation of Claudin-5 protein in mouse brain endothelial cells.

524 (**A**) Transendothelial electrical resistance (TEER) of primary mouse brain endothelial cells
525 (mBECs) transfected with either an siRNA targeting Rab7a (siRab7a), or a scrambled siRNA
526 (siCTRL) in the absence or presence of inflammatory cytokines (TNFα, IL-1β 10 ng/mL). The
527 gray area represents the period of time during which cells were treated with cytokines or vehicle.
528 (**B, C**) Quantification of the area under the curve (A.U.C.) during treatment with cytokines [gray
529 area in (a)] and of the percentage of TEER reduction 48 hours after treatment with cytokines (right
530 panel). Each dot represents an independent experiment. Data are means ± s.e.m. **: $p<0.01$; *:
531 $p<0.05$; n.s. $p>0.05$; one-way ANOVA with post-hoc Tukey's correction (left graph), and
532 Student's t-test (right graph). (**D**) Western blot for junctional proteins ZO-1, Occludin and Claudin-
533 5 in siCTRL- and siRab7a-transfected mBECs with or without cytokines. β-actin serves as control.
534 The molecular weights of the proteins are shown on the right. (**E-G**) Quantification of Claudin-5,
535 Occludin and ZO-1 levels in siCTRL- and siRab7a-transfected with or without cytokines. Each
536 dot represents an independent experiment (n=4). Data are means ± s.e.m.; ***: $p<0.001$; **:
537 $p<0.01$; *: $p<0.05$; n.s. $p>0.05$; one-way ANOVA with post-hoc Tukey's correction. (**H-K"**)
538 Immunofluorescence for Claudin 5 (green) and ZO-1 (red) in mBECs transfected with either
539 siCTRL (**H-I"**) or siRab7a (**J-K"**) in the presence or absence of cytokines. Cytokine treatment
540 induces fewer structural abnormalities in Claudin-5 localization at cell junctions of siRab7a-treated
541 mBECs. (**L**) Working model for the role of Rab7a in tight junction instability after ischemic stroke.
542 In healthy conditions, Rab7a cycles equally between its active and inactive states, balancing the
543 rates of degradation and recycling of internalized membrane proteins including adherens and tight
544 junction proteins. Under pathological conditions, such as ischemic stroke, some inflammatory
545 cytokines (e.g. IL-1β, TNFα) induce Ccz1, a GEF that activates Rab7a. The hyperactivated Rab7a

546 increases the rate of degradation of junctional proteins leading to increased paracellular BBB

547 permeability. Please see also **Figures S4** and **S5**.

548

549 **REFERENCES**

550 1. Liebner, S. *et al.* Functional morphology of the blood-brain barrier in health and disease.
551 *Acta Neuropathol* **135**, 311-336 (2018).

552 2. Bamford, J., Sandercock, P., Dennis, M., Burn, J. & Warlow, C. A prospective study of
553 acute cerebrovascular disease in the community: the Oxfordshire Community Stroke
554 Project--1981-86. 2. Incidence, case fatality rates and overall outcome at one year of
555 cerebral infarction, primary intracerebral and subarachnoid haemorrhage. *J Neurol*
556 *Neurosurg Psychiatry* **53**, 16-22 (1990).

557 3. Bonita, R., Solomon, N. & Broad, J.B. Prevalence of stroke and stroke-related disability.
558 Estimates from the Auckland stroke studies. *Stroke* **28**, 1898-1902 (1997).

559 4. Kammersgaard, L.P. *et al.* Short- and long-term prognosis for very old stroke patients. The
560 Copenhagen Stroke Study. *Age Ageing* **33**, 149-154 (2004).

561 5. Rothwell, P.M. *et al.* Population-based study of event-rate, incidence, case fatality, and
562 mortality for all acute vascular events in all arterial territories (Oxford Vascular Study).
563 *Lancet* **366**, 1773-1783 (2005).

564 6. Kaur, C. & Ling, E.A. Blood brain barrier in hypoxic-ischemic conditions. *Current*
565 *neurovascular research* **5**, 71-81 (2008).

566 7. Sandoval, K.E. & Witt, K.A. Blood-brain barrier tight junction permeability and ischemic
567 stroke. *Neurobiol Dis* **32**, 200-219 (2008).

568 8. Arai, K., Jin, G., Navaratna, D. & Lo, E.H. Brain angiogenesis in developmental and
569 pathological processes: neurovascular injury and angiogenic recovery after stroke. *The*
570 *FEBS journal* **276**, 4644-4652 (2009).

571 9. Hawkins, B.T. & Davis, T.P. The blood-brain barrier/neurovascular unit in health and
572 disease. *Pharmacological reviews* **57**, 173-185 (2005).
573 10. Knowland, D. *et al.* Stepwise recruitment of transcellular and paracellular pathways
574 underlies blood-brain barrier breakdown in stroke. *Neuron* **82**, 603-617 (2014).
575 11. Lutz, S.E. *et al.* Caveolin1 Is Required for Th1 Cell Infiltration, but Not Tight Junction
576 Remodeling, at the Blood-Brain Barrier in Autoimmune Neuroinflammation. *Cell Rep* **21**,
577 2104-2117 (2017).
578 12. Doll, D.N., Barr, T.L. & Simpkins, J.W. Cytokines: their role in stroke and potential use
579 as biomarkers and therapeutic targets. *Aging Dis* **5**, 294-306 (2014).
580 13. Rayasam, A. *et al.* Immune responses in stroke: how the immune system contributes to
581 damage and healing after stroke and how this knowledge could be translated to better
582 cures? *Immunology* **154**, 363-376 (2018).
583 14. Iadecola, C., Buckwalter, M.S. & Anrather, J. Immune responses to stroke: mechanisms,
584 modulation, and therapeutic potential. *J Clin Invest* **130**, 2777-2788 (2020).
585 15. Doyle, K.P. & Buckwalter, M.S. Immunological mechanisms in poststroke dementia. *Curr*
586 *Opin Neurol* **33**, 30-36 (2020).
587 16. Endres, M. *et al.* Immune Pathways in Etiology, Acute Phase, and Chronic Sequelae of
588 Ischemic Stroke. *Circ Res* **130**, 1167-1186 (2022).
589 17. Stamatovic, S.M., Keep, R.F., Wang, M.M., Jankovic, I. & Andjelkovic, A.V. Caveolae-
590 mediated internalization of occludin and claudin-5 during CCL2-induced tight junction
591 remodeling in brain endothelial cells. *J Biol Chem* **284**, 19053-19066 (2009).
592 18. Marchiando, A.M. *et al.* Caveolin-1-dependent occludin endocytosis is required for TNF-
593 induced tight junction regulation in vivo. *J Cell Biol* **189**, 111-126 (2010).

594 19. Drab, M. *et al.* Loss of caveolae, vascular dysfunction, and pulmonary defects in caveolin-
595 1 gene-disrupted mice. *Science* **293**, 2449-2452 (2001).
596 20. Razani, B. *et al.* Caveolin-1 null mice are viable but show evidence of hyperproliferative
597 and vascular abnormalities. *J Biol Chem* **276**, 38121-38138 (2001).
598 21. Jasmin, J.F. *et al.* Caveolin-1 deficiency increases cerebral ischemic injury. *Circ Res* **100**,
599 721-729 (2007).
600 22. Li, X., Garrity, A.G. & Xu, H. Regulation of membrane trafficking by signalling on
601 endosomal and lysosomal membranes. *J Physiol* **591**, 4389-4401 (2013).
602 23. Zerial, M. & McBride, H. Rab proteins as membrane organizers. *Nat Rev Mol Cell Biol* **2**,
603 107-117 (2001).
604 24. Zhang, M., Chen, L., Wang, S. & Wang, T. Rab7: roles in membrane trafficking and
605 disease. *Biosci Rep* **29**, 193-209 (2009).
606 25. Gutierrez, M.G., Munafo, D.B., Beron, W. & Colombo, M.I. Rab7 is required for the
607 normal progression of the autophagic pathway in mammalian cells. *J Cell Sci* **117**, 2687-
608 2697 (2004).
609 26. Edinger, A.L., Cinalli, R.M. & Thompson, C.B. Rab7 prevents growth factor-independent
610 survival by inhibiting cell-autonomous nutrient transporter expression. *Developmental cell*
611 **5**, 571-582 (2003).
612 27. Romero Rosales, K., Peralta, E.R., Guenther, G.G., Wong, S.Y. & Edinger, A.L. Rab7
613 activation by growth factor withdrawal contributes to the induction of apoptosis. *Mol Biol*
614 *Cell* **20**, 2831-2840 (2009).

615 28. Ceresa, B.P. & Bahr, S.J. rab7 activity affects epidermal growth factor:epidermal growth
616 factor receptor degradation by regulating endocytic trafficking from the late endosome. *J*
617 *Biol Chem* **281**, 1099-1106 (2006).
618 29. Peralta, E.R., Martin, B.C. & Edinger, A.L. Differential effects of TBC1D15 and
619 mammalian Vps39 on Rab7 activation state, lysosomal morphology, and growth factor
620 dependence. *J Biol Chem* **285**, 16814-16821 (2010).
621 30. Roy, S.G., Stevens, M.W., So, L. & Edinger, A.L. Reciprocal effects of rab7 deletion in
622 activated and neglected T cells. *Autophagy* **9**, 1009-1023 (2013).
623 31. Nordmann, M. *et al.* The Mon1-Ccz1 Complex Is the GEF of the Late Endosomal Rab7
624 Homolog Ypt7. *Current Biology* **20**, 1654-1659 (2010).
625 32. Kinchen, J.M. & Ravichandran, K.S. Identification of two evolutionarily conserved genes
626 regulating processing of engulfed apoptotic cells. *Nature* **464**, 778-782 (2010).
627 33. Poteryaev, D., Datta, S., Ackema, K., Zerial, M. & Spang, A. Identification of the Switch
628 in Early-to-Late Endosome Transition. *Cell* **141**, 497-508 (2010).
629 34. Langemeyer, L. *et al.* A conserved and regulated mechanism drives endosomal Rab
630 transition. *Elife* **9** (2020).
631 35. Kiontke, S. *et al.* Architecture and mechanism of the late endosomal Rab7-like Ypt7
632 guanine nucleotide exchange factor complex Mon1–Ccz1. *Nature Communications* **8**,
633 14034 (2017).
634 36. Jopling, H.M. *et al.* Rab GTPase regulation of VEGFR2 trafficking and signaling in
635 endothelial cells. *Arterioscler Thromb Vasc Biol* **29**, 1119-1124 (2009).

636 37. Kofler, N. *et al.* The Rab-effector protein RABEP2 regulates endosomal trafficking to
637 mediate vascular endothelial growth factor receptor-2 (VEGFR2)-dependent signaling. *J*
638 *Biol Chem* **293**, 4805-4817 (2018).
639 38. Okon, I.S. *et al.* Protein kinase LKB1 promotes RAB7-mediated neuropilin-1 degradation
640 to inhibit angiogenesis. *The Journal of clinical investigation* **124**, 4590-4602 (2014).
641 39. Chichger, H., Braza, J., Duong, H., Boni, G. & Harrington, E.O. Select Rab GTPases
642 Regulate the Pulmonary Endothelium via Endosomal Trafficking of Vascular Endothelial-
643 Cadherin. *Am J Respir Cell Mol Biol* **54**, 769-781 (2016).
644 40. Nitta, T. *et al.* Size-selective loosening of the blood-brain barrier in claudin-5-deficient
645 mice. *J Cell Biol* **161**, 653-660 (2003).
646 41. Jiang, S.X. *et al.* Chlortetracycline and demeclocycline inhibit calpains and protect mouse
647 neurons against glutamate toxicity and cerebral ischemia. *J Biol Chem* **280**, 33811-33818
648 (2005).
649 42. Cantalupo, G., Alifano, P., Roberti, V., Bruni, C.B. & Bucci, C. Rab-interacting lysosomal
650 protein (RILP): the Rab7 effector required for transport to lysosomes. *EMBO J* **20**, 683-
651 693 (2001).
652 43. Clarkson, B.D. *et al.* T cell-derived interleukin (IL)-21 promotes brain injury following
653 stroke in mice. *J Exp Med* **211**, 595-604 (2014).
654 44. Li, L., Lou, W., Li, H., Zhu, Y. & Huang, X. Upregulated C-C Motif Chemokine Ligand 2
655 Promotes Ischemic Stroke via Chemokine Signaling Pathway. *Ann Vasc Surg* **68**, 476-486
656 (2020).

657 45. Lin, Y. *et al.* Critical role of astrocytic interleukin-17 A in post-stroke survival and
658 neuronal differentiation of neural precursor cells in adult mice. *Cell Death & Disease* **7**,
659 e2273-e2273 (2016).
660 46. Kuchitsu, Y. & Fukuda, M. Revisiting Rab7 Functions in Mammalian Autophagy: Rab7
661 Knockout Studies. *Cells* **7** (2018).
662 47. Umeda, K. *et al.* ZO-1 and ZO-2 independently determine where claudins are polymerized
663 in tight-junction strand formation. *Cell* **126**, 741-754 (2006).
664 48. Liu, J., Jin, X., Liu, K.J. & Liu, W. Matrix metalloproteinase-2-mediated occludin
665 degradation and caveolin-1-mediated claudin-5 redistribution contribute to blood-brain
666 barrier damage in early ischemic stroke stage. *J Neurosci* **32**, 3044-3057 (2012).
667 49. Underly, R.G. *et al.* Pericytes as Inducers of Rapid, Matrix Metalloproteinase-9-Dependent
668 Capillary Damage during Ischemia. *J Neurosci* **37**, 129-140 (2017).
669 50. Abdullah, Z., Rakkar, K., Bath, P.M. & Bayraktutan, U. Inhibition of TNF-alpha protects
670 in vitro brain barrier from ischaemic damage. *Mol Cell Neurosci* **69**, 65-79 (2015).
671 51. Shi, Y. *et al.* Endothelium-targeted overexpression of heat shock protein 27 ameliorates
672 blood-brain barrier disruption after ischemic brain injury. *Proc Natl Acad Sci U S A* **114**,
673 E1243-E1252 (2017).
674 52. Agola, J.O. *et al.* A competitive nucleotide binding inhibitor: in vitro characterization of
675 Rab7 GTPase inhibition. *ACS Chem Biol* **7**, 1095-1108 (2012).
676 53. Wang, Y. *et al.* Ephrin-B2 controls VEGF-induced angiogenesis and lymphangiogenesis.
677 *Nature* **465**, 483-486 (2010).

678 54. Arac, A. *et al.* Systemic augmentation of alphaB-crystallin provides therapeutic benefit
679 twelve hours post-stroke onset via immune modulation. *Proc Natl Acad Sci U S A* **108**,
680 13287-13292 (2011).
681 55. Mazzoni, J. *et al.* The Wnt Inhibitor Apcdd1 Coordinates Vascular Remodeling and Barrier
682 Maturation of Retinal Blood Vessels. *Neuron* **96**, 1055-1069 e1056 (2017).
683
684

685 **STAR ★ METHODS**

686 Detailed methods are provided in the online version of this paper and include the following:

687 KEY RESOURCES TABLE

688 RESOURCE AVAILABILITY

689 - Lead contact
690 - Materials availability
691 - Data and code availability

692 EXPERIMENTAL MODEL AND SUBJECT DETAILS

693 - Mice

694 METHOD DETAILS

695 - Mouse ischemic stroke model
696 - Biocytin-TMR and serum IgG permeability analysis
697 - Immunofluorescence
698 - Western blotting
699 - mBEC culture and Rab7a silencing *in vitro*
700 - Rab7a-GTP pull down assay
701 - Trans-endothelial electrical resistance
702 - *In vitro* assays with primary mouse BECs

703 QUANTIFICATION AND STATISTICAL ANALYSIS

704 - Image acquisition and quantification
705 - Statistical analysis

706

707

708 **STAR ★ METHODS**

709 **KEY RESOURCES TABLE**

Reagent or resource	Source	Identifier
Primary antibodies		
Rabbit anti-Rab7a	Abcam	Cat #ab137029 RRID: AB_2629474
Mouse anti-ZO-1	Thermo Fisher Scientific	Cat #33-9100, RRID: AB_2533147
Rabbit anti-ZO-1	Thermo Fisher Scientific	Cat# 61-7300, RRID: AB_2533938
Rabbit anti-GLUT1	Millipore	Cat# 07-1401, RRID: AB_1587074
Rabbit anti-Claudin-5	Thermo Fisher Scientific	Cat #34-1600, RRID: AB_2533157
Rabbit anti-VE-cadherin	Abcam	Cat# ab33168, RRID: AB_870662
Rat anti-CD68	Abcam	Cat# ab53444, RRID: AB_869007
Rabbit anti-Iba1	FUJIFILM Wako Shibayagi	Cat# 019-19741, RRID: AB_839504
Mouse anti-NeuN	Sigma-Aldrich	Cat #MAB377, RRID: AB_2298772
Mouse anti-Beta-actin	Novus	Cat# NB600-501,

		RRID: AB_10077656
Rabbit anti-Caveolin 1	Abcam	Cat# ab18199, RRID: AB_444314
Mouse anti-GST	Santa Cruz Biotechnology	Cat# sc-57590, RRID: AB_783590
Rabbit anti-Occludin	Thermo Fisher Scientific	Cat# 71-1500, RRID: AB_2533977
Rabbit anti-Ccz1	Abcam	Cat# ab131311, RRID: AB_11158512
Rabbit anti-EEA1	Abcam	Cat# ab2900, RRID: AB_2262056
Rabbit anti-LAMP1	Abcam	Cat# ab24170, RRID: AB_775978
Rabbit anti-ATG5	Cell Signaling Technology	Cat# 12994, RRID: AB_2630393
Rabbit anti-p62	Abcam	Cat# ab109012, RRID: AB_2810880
Chemicals, peptides, and recombinant proteins		
Biocytin-TMR (5-(and-6)-tetramethylrhodamine biocytin)	ThermoFisher Scientific	Cat #T12921
Albumin from Bovine Serum (BSA), AlexaFluor™ 594 conjugate	ThermoFisher Scientific	Cat #A13101

Griffonia (Bandeiraea) Simplicifolia Lectin I (GSL I, BSL I), Rhodamine	Vector Labs	Cat #RL-1102-2
Lipofectamine™ 2000 Transfection Reagent	Invitrogen	Cat #11668019
Recombinant Mouse TNFα	R&D systems	Cat # 410-MT
Recombinant Mouse IL-1β	R&D systems	Cat #401-ML
LysoTracker™ Red	Thermo Fisher Scientific	Cat #L7528
Experimental Models		
C57BL/6 mouse primary brain microvascular endothelial cells	Cell Biologics	Cat #C57-6023
Rab7a$^{flox/flox}$	Dr. Aimee Edinger	RRID: IMSR_JAX:021589
Cdh5(PAC)-Cre^{ERT2} *(VEC-PAC)*	Gift from Dr. Jan Kitajewski	RRID: IMSR_GPT:T052686
Tg(eGFP-Claudin5)		Published in [10]
Plasmids		
pGEX-4T-3-mR7BD	Addgene	Cat #79149, RRID: Addgene_79149
Oligonucleotides		
Rab7a Stealth siRNA MSS276704, MSS276705, MSS276706	Invitrogen	Cat #1320001

Stealth RNAi™ siRNA Negative Control Med GC Duplex #3	Invitrogen	Cat #12935113
Rab7a flox forward: 5'-CTCACTCACTCCTAAATGG-3’	IDT	N/A
Rab7a flox reverse: 5'-TTAGGCTGTATGTATGTGC-3’	IDT	N/A
Rab7a null forward: 5'-GGGCTGCAGGAATTCGGATAAC-3’	IDT	N/A
Rab7a null reverse: 5'-CATGGTAACAAGTCTGTCGTCC-3’	IDT	N/A
Cre forward: 5'-GCTAAGTGCCTTCTCTACACCTGC-3’	IDT	N/A
Cre reverse: 5'- GGAAAATGCTTCTGTCCGTTTG -3’	IDT	N/A
GFP forward: 5'-CCCTGAAGTTCATCTGCACCAC-3’	IDT	N/A
GFP reverse: 5'-TTCTCGTTGGGGTCTTTGCTC-3’	IDT	N/A
Software and algorithms		
Zen microscopy software	Zeiss	RRID:SCR_013672
Prism 9	GraphPad	RRID: SCR_002798

Empiria Studio	LI-COR	RRID: SCR_022512
ImageJ/Fiji	NIH	RRID: SCR_002285

710

711 **RESOURCE AVAILABILITY**

712 **Lead contact**

713 Further information and requests for resources and reagents should be directed to the lead contact,
714 Dritan Agalliu (da191@cumc.columbia.edu).

715

716 **Materials availability**

717 This study did not generate new unique reagents.

718

719 **Data and code availability**

720 All data are available in the manuscript and the supplementary information. The codes used in this
721 study have been previously published and are freely available (see Key Resources Table). Any
722 additional information required to reanalyze the data reported in this study will be available upon
723 request.

724

725 **EXPERIMENTAL MODEL AND SUBJECT DETAILS**

726 **Mice**

727 All experimental procedures were approved by the IACUC committees at the University of
728 California, Irvine and Columbia University Irving Medical Center. The following mouse strains
729 were used: *Tg(eGFP-Claudin5)* [10]; *Rab7a*$^{flox/flox}$ [30]; *Cdh5(PAC)-Cre*^{ERT2} *(VEC-PAC)* [53], kindly
730 provided by Dr. Jan Kitajewski (Columbia University Irving Medical Center, New York, US). To

731 induce Cre^{ERT2}-mediated recombination, 4-OH-tamoxifen (Sigma-Aldrich) was dissolved in 10%
732 ethanol/corn oil mixture to a final concentration of 2 mg/ml, and administered by intraperitoneal
733 injections at a dose of 35 µg/g body weight for 5 consecutive days starting at postnatal day P1 and
734 5 as well as 5 consecutive days in the adult ending one week before the t-MCAO procedure.
735

736 **METHOD DETAILS**

737 **Mouse ischemic stroke model**

738 Ischemic stroke was induced in 10-14 weeks old male mice by t-MCAO for 45 minutes as
739 described [54]. Briefly, mice were anesthetized with 1.5-2% isoflurane, left external and common
740 carotid artery were ligated and a 7-0 silicon rubber-coated monofilament (Doccol) was inserted
741 through the common carotid artery into the internal carotid artery. Reperfusion was obtained by
742 removing the monofilament 45 minutes after its insertion. The body temperature of the mice was
743 monitored and maintained at 37°C throughout the procedure. The neurological deficits in mice
744 after t-MCAO were evaluated and scored as described in Jiang S.X. et al., 2005 [41].
745

746 **Biocytin-TMR and serum IgG permeability analysis**

747 Mice received a tail vein injection of 100 µl of Biocytin-TMR (1% in PBS; ThermoFisher
748 Scientific). The dye was allowed to circulate for 30 minutes. Animals were anesthetized with
749 isoflurane and perfused first with PBS, then with 4% PFA in PBS. AlexaFluor 488-conjugated
750 goat anti-mouse IgG (Invitrogen, 1:500) was used to visualize serum IgG leakage in brain sections.
751

752 **Immunofluorescence**

753 After dissection, PFA-perfused brains and livers were fixed in 4% PFA at 4°C for 6 hours, then
754 cryoprotected in 30% sucrose and embedded in Tissue-Tek OCT. For immunofluorescence
755 staining for Rab7a, Claudin-5 and ZO-1, brains were dissected after perfusion with PBS, fresh-
756 frozen in Tissue-Tek and sections were fixed with cold 95% ethanol for 30 minutes and acetone
757 for 1 minute followed by three 5-minute washes with PBS. Brains were sectioned in 12 μm-thick
758 coronal slices spanning all bregma regions of interest using a Leica cryostat. For primary mBECs
759 cultures, cells were fixed with cold 95% ethanol for 30 minutes and acetone for 1 minute followed
760 by three 5-minute washes with PBS. The following primary antibodies were used: rabbit anti-
761 Rab7a (1:100, Abcam), rabbit anti-ZO-1 (1:500, Invitrogen), rabbit anti-GLUT1 (1:200, Thermo
762 Scientific), rabbit anti-Claudin5 (1:500, Invitrogen), rabbit anti-VE-cadherin (1:250, Abcam), rat
763 anti-CD68 (1:500, Abcam), rabbit anti-Iba1 (1:1000, Wako), mouse anti-NeuN (1:500, Millipore).
764 BSL-rhodamine (1:250, Vector Laboratories) was used to label the vasculature.
765

766 **Western blotting**

767 Protein levels for endothelial markers were assessed using the Odyssey Sa infrared imaging system
768 (LI-COR). β-actin was used as housekeeping gene. The following primary antibodies were used:
769 mouse anti-Claudin5 (1:500, Invitrogen), rabbit anti-Caveolin-1 (1:2000, Abcam), rabbit anti-
770 Occludin (1:2000, Invitrogen), rabbit anti-VE-cadherin (1:2000, Abcam), mouse anti-ZO-1
771 (1:2000, Thermo Scientific), rabbit anti-Rab7a (1:1000, Abcam), mouse anti-GST (1:1000, Santa
772 Cruz), rabbit anti-Ccz1 (1:1000, Abcam), rabbit anti-EEA1 (1:2000, Abcam), rabbit anti-LAMP1
773 (1:1000, Abcam), mouse anti-β-actin (1:5000, Novus Biologicals), p62 (1:10000, Abcam) and
774 Atg5 (1:500, Cell Signaling). IR-Dyes 680 and 800 (1:10000, LI-COR) were used as secondary
775 antibodies. Protein expression levels were quantified using the Empiria Studio software (LI-COR),

776 normalized on their respective β-actin expression values and presented as a percentage of protein
777 levels in control conditions.
778
779 **mBEC culture and Rab7a silencing *in vitro***
780 Primary mBECs were purchased from Cell Biologics and grown in endothelial cell medium
781 supplemented with growth factors and 5% FBS (Cell Biologics). Stealth RNAi duplexes targeting
782 Rab7a were purchased from Invitrogen. Stealth RNAi negative control Med CG Duplex #3
783 (Invitrogen) was used as negative control in all experiments. 12.5 nM of siRNA was transfected
784 using Lipofectamine 2000 (Invitrogen), following the manufacturer's instructions.
785
786 **Rab7a-GTP pull-down assay**
787 The plasmid pGEX-4T-3-mR7BD, which expresses a recombinant protein consisting of the Rab7a
788 binding domain of the murine RILP protein fused to the C terminus of GST (Addgene, cat#79149),
789 was transformed into Escherichia coli strain BL21. The transformed bacteria were induced to
790 express the GST-RILP protein, which was then purified from the bacterial cell lysates using
791 glutathione-Sepharose 4B beads (GE Healthcare) as described [27]. Control and cytokine/OGD
792 treated mBECs were lysed in pull-down buffer (20 mM HEPES, 100 mM NaCl, 5 mM $MgCl_2$, 1%
793 TX-100, and protease inhibitors) and sonicated. Protein levels in the mBEC lysates were quantified
794 via the BCA assay. Each pull-down was performed by incubating 30 µl of the GST-RILP bound
795 bead slurry pre-equilibrated in pull-down buffer with 300 µg of cell lysate, and rocking the bead-
796 lysate mixture in a nutator overnight at 4°C. Afterwards, the beads were washed thrice with cold
797 pull-down buffer, and bound proteins were eluted by adding sample loading buffer with SDS and
798 incubating at 95°C for 10 min.

799

800 **Trans-endothelial electrical resistance**

801 mBECs transfected with either siCTRL or siRab7a were plated on poly-D-lysine and collagen IV-
802 coated gold-electrode array 96-well plates (Applied Biophysics) and grown to confluency. They
803 were then switched to low serum medium (1% FBS) for 24 hours and treated with TNFα and IL1β
804 as described above. The electrical resistance of the cultures was recorded every 20 minutes for the
805 duration of the experiment using an ECIS Z- θ system (Applied Biophysics). GraphPad Prism was
806 used to generate resistance curves and to calculate the area under the curve for each experimental
807 condition, as previously described [55].

808

809 ***In vitro* assays with primary mouse BECs**

810 For both albumin uptake and Lysotracker assays, mBECs were grown to confluency on poly-D-
811 lysin- and collagen IV-coated glass-bottom 24-well plates (Greiner Bio-One), switched to low
812 serum (1% FBS) medium and treated with TNFα and IL1β as described above. Cells were
813 incubated with either AlexaFluor 594-albumin (100 μg/ml; Thermo Fisher Scientific) or
814 Lysotracker (50 nM; Thermo Fisher Scientific) for 1 hour at 37º C, washed with PBS and fixed in
815 4% PFA.

816

817 **QUANTIFICATION AND STATISTICAL ANALYSIS**

818 **Image acquisition and quantification**

819 Images of the whole brain sections were acquired with a Zeiss Axioimager fluorescence
820 microscope, higher resolution images were acquired using a Zeiss LSM700 confocal microscope.
821 For comparison purposes, all images of the same staining were acquired under the same settings.

822 All images were processes using Fiji, and all quantifications were carried out blinded. The areas
823 of Biocytin-TMR or IgG leakage were quantified by uniformly thresholding the brain sections and
824 measuring the area exceeding the threshold in each section. The volume of the leakage was
825 calculated as the product of cross-sectional areas and distance between sections. Intensity of the
826 leakage was determined by sampling identical regions in contralateral and ipsilateral cortex in each
827 animal, normalizing their fluorescence intensity on the average fluorescence intensity of the liver
828 from the same animal and calculating the ratio between the ipsilateral and the contralateral cortex.
829 To quantify junctional abnormalities, junctional strands, gaps and protrusions were identified as
830 described before [10] and the percentage of junctional gaps or protrusion over the total number of
831 junctional strands was calculated. To quantify neuronal viability, we calculated the ratio of NeuN
832 positive cells over the total of cells for each field of view. Albumin uptake and Lysotracker *in vitro*
833 were quantified by measuring the area covered by albumin or lysotracker respectively, and
834 dividing it by the number of cells in the field, as previously described [55].
835

836 **Statistical analyses**

837 All statistical analyses were performed using GraphPad Prism version 8.1 or higher. Unless
838 differently specified in the figure legend, data are represented as mean ± s.e.m.. The Shapiro-Wilk
839 test was used to verify the normality of datasets. For dataset showing normal distribution, pairwise
840 comparisons were performed using a two-tailed Student's t-test and multiple comparisons were
841 performed using one-way ANOVA with post-hoc Tukey's correction. P values lower than 0.05
842 were considered statistically significant (***: $p<0.001$; **: $p<0.01$; *: $p<0.05$).